metals

MDPI

Article

Characterization of Solid-Solution and Aging Process in Mg-5 wt.%Sn Alloy

Yongjun Liu and Hongmei Liu *

Key Laboratory of Advanced Technologies of Materials, Ministry of Education, School of Materials Science and Engineering, Southwest Jiaotong University, Chengdu 610032, China
* Correspondence: lhm@home.swjtu.edu.cn

Abstract: Firstly, the properties and the microstructure evolution of the solid-solution process of Mg-5 wt.%Sn were studied. From the motion analysis of resistivity and microhardness during solution treatment, the reasonable solution technology of Mg-5 wt.%Sn should be 12–16 h at 480 °C. After solution treatment at 480 °C for 16 h, the precipitating behavior in supersaturated solid solution. Mg-5 wt.%Sn alloy was investigated. In the aging process, it was observed that there were precipitated phases in the both grain and grain boundaries, and continuous inhomogeneous precipitation occurred along the grain boundaries, and continuous homogeneous precipitation happened in the grain. Transmission Electron Microscope (TEM) analysis indicated the plate- and lath-shaped precipitates within the grains and only the plate-shaped precipitates along the grain boundary. High-Resolution Electron Microscopy (HRTEM) studies have shown that metastable precipitates may occur during aging, coherently or semi-coherent with the matrix. Energy Dispersive Analysis by X-ray (EDAX) analysis showed that the Mg/Sn ratio was not actually constant, and the Sn content of the metastable phase was lower than that of the Mg_2Sn equilibrium phase. X-ray diffraction (XRD) studies confirm the existence of this metastable phase, which is supposed to be GP zone and metastable Mg_3Sn phase.

Keywords: magnesium alloys; tin; solid-solution; ageing; HRTEM; metastable phase

Citation: Liu, Y.; Liu, H. Characterization of Solid-Solution and Aging Process in Mg-5 wt.%Sn Alloy. *Metals* **2023**, *13*, 807. https://doi.org/10.3390/met13040807

Academic Editor: Andrey Belyakov

Received: 29 March 2023
Revised: 15 April 2023
Accepted: 17 April 2023
Published: 20 April 2023

1. Introduction

The Mg-Sn alloys are known as an age hardenable system [1–3], in which the solubility of Sn in α-Mg solid solution drops sharply from 14.85 wt.% at the eutectic transformation temperature 561 °C to 0.45 wt.% at 200 °C. This provides a fundamental basis for improving the mechanical properties of these alloys through solid-solution ageing treatment [1–3]. The Mg_2Sn precipitate (FCC, a = 0.676 nm, space group $m\bar{3}m$) in Mg-Sn alloys has a high melting temperature (~771.5 °C), which is higher than that of $Mg_{17}Al_{12}$ (462 °C) in Mg-Al alloys and MgZn (347 °C) in Mg-Zn alloys. In addition, the maximum solidification temperature range of Mg-Sn binary alloys is about 67 °C, which is much narrower compared with 136 °C and 283 °C of Mg-Al and Mg-Zn binary alloys respectively. As a result, the casting defects such as dispersed shrinkage and hot tearing in Mg-Sn alloys are less severe than that in Mg-Al and Mg-Zn alloys. After 2000 there has been a renewed global interest in these alloys which are believed to have potential applications at elevated temperatures [3–21]. The age hardening behavior of the Mg-Sn system alloy was first reported by Derge et al. [22] who suggested in aged magnesium-tin alloys the Mg~Sn precipitates lie mainly parallel to the (0001) plane of the matrix [22]. Van Der Planken [23] examined the orientation relationship between the Mg matrix and the Mg_2Sn equilibrium phase using X-ray diffraction and optical microscopy techniques, and reported that the Mg_2Sn phase formed a plate-like morphology and various orientation relationships were observed depending on the formation temperature. At temperatures around 200 °C, the plate-like Mg_2Sn particles were reported to form on the (0001)Mg basal planes of the matrix with the following orientation relationship: $(111)_p//(0001)_m$, $<110>_p//<11\bar{2}0>_m$. Henes [12]

also reported that the Mg_2Sn in the binary Mg-Sn alloy has the orientation relationships of $(110)_p//(0001)_m$, $<001>_p//<11\bar{2}0>$ and $(110)_p//(0001)_m$, $<\bar{1}11>_p//<11\bar{2}0>_m$ at an ageing temperature of 130 to 200 °C and $(11\,1)_p//(0001)_m$, $<\bar{1}01>_p//<11\bar{2}0>$ and $(11\,1)_p//(0001)_m$, $<1\bar{1}2>_p//<11\bar{2}0>_m$ at an ageing temperature of 200 to 300 °C. This orientation relationship and the plate-like morphology were confirmed by Mendis [14] and Sasaki et al. [15]. Understanding the development of precipitation in Mg-Sn binary alloys is important, since this form of precipitation is responsible for most of the age hardening in Mg-Sn based alloys. Henes [24] was the first to find the metastable structure in Mg-Sn except for the investigative results from, whose study indicated that the precipitation was preceded by formation of short-range order in aged magnesium-tin alloys. The metastable phase was confirmed in and in Mg-9.8 wt.%Sn [25] and Mg-7 wt.%Sn [26] alloys. The aim of this paper is to further study the metastable precipitate as a basis for improving the age-hardening response of these alloys in the future.

2. Experimental

Mg-5 wt.%Sn alloy was prepared by melting pure Mg 99.95 wt.% and Sn99.98 wt.% in MgO refractory crucible and under the protection of RJ-2 melting agent. Manual stirring was applied at 30 strokes/min for 3 min during alloying. Plate samples with dimensions of 140 × 110 × 20 mm^3 were cast by pouring the melt at 720 °C into a grey cast iron mold (30-mm wall thickness) preheated to 250 °C.

Mg-5 wt.%Sn alloy was solution treated at 480 °C, maintained for different times under the protection of the troilite, and then water quenched. The change of electrical resistivity of 2 × 2 × 100 mm^3 samples was measured using a custom-built rig based on the four-point probe technique. The applied current was approximately 20 mA, reversed at a rate of 30 Hz. All measurements were conducted with the specimen immersed in water to minimize the effect of temperature.

Vickers hardness was measured under the HD-1000TM digital microhardness tester with a load of 50 grams and a loading duration of 10 s. For each specimen, at least 10 indents were performed and the average values were used.

After solution treatment at 480 °C for 16 h, the precipitating behavior in supersaturated solid solution of Mg-5 wt.%Sn alloy was investigated. The ageing treatment was conducted at 160 °C and 240 °C for different time, also under the protection of the troilite.

Samples for metallographic characterization were sliced at 1/3 of the cast sample height. They were ground, polished and etched with a solution of 20 vol.% nitric acid + ethyl alcohol. The microstructures were characterized using optical microscopy (OLYMPUS-BH-2). The overall phase structures of the test alloys were analyzed using X-ray diffraction (D/Max2rA) with Cu Kα radiation.

Transmission electron microscope (TEM) specimens were prepared by ion-milling using the Precision Ion Polishing System (GATAN691). High-resolution electron microscopy (HRTEM) observation was carried out using JEM-2010UHR at 200 kV and Energy Dispersive X-ray was recorded using NORAN VANTAGE DS.

3. Results and Analysis

3.1. Characterization of Solid-Solution Process in Mg-5 wt.%Sn Alloy

3.1.1. Electrical Resistivity

The change in electrical resistivity of Mg-5 wt.%Sn in the solution process is shown in Figure 1. The measured resistivity of as-cast of Mg-5 wt.%Sn is 0.087 μΩ·m, which is close to its value of 0.089 μΩ·m form the work of F. Pan et al. [27,28]. It can be seen from Figure 1 that the resistivity first increases and then decreases with the solution time, and the resistivity reaches a maximum of 0.099 μΩ·m at 10 h, which is an increase of 14.2% compared with the cast sample. In the work of F. Pan [28], the resistivity of Mg-5wt.%Sn in the solid solution state is 15.3% higher than that of the as-cast Mg-5wt.%Sn, which is consistent with the results of this work.

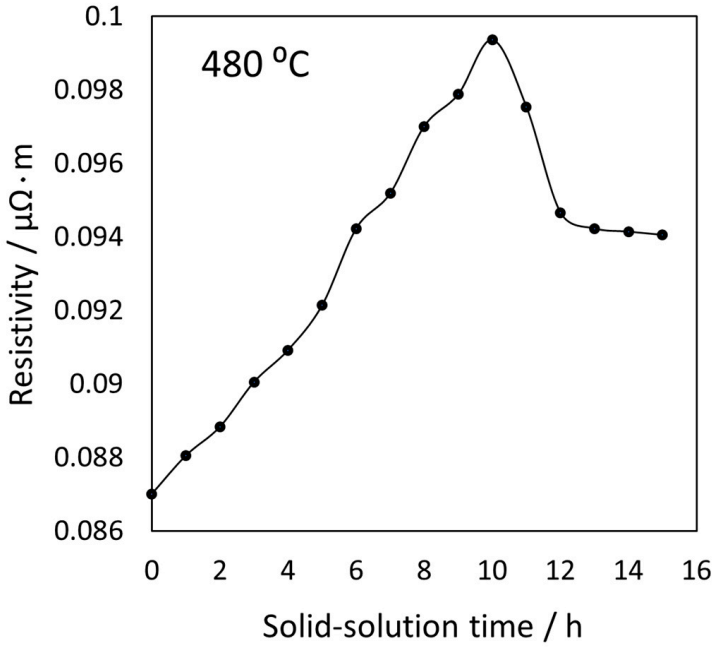

Figure 1. The resistivity of Mg-5 wt.%Sn alloy changes with the solution time during solution treatment at 480 °C.

When the solid-solution time is over 12 h, the change of the electrical resisitivity is unobvious. According to the Matthiessen theory, the resistivity can be given by:

$$\rho = \rho_0 + \Delta\rho_S + \Delta\rho_P + \Delta\rho_V + \Delta\rho_D + \Delta\rho_{GB} \quad (1)$$

where $\Delta\rho_S$ is the variable of resisitivity caused by the solid-solution, and $\Delta\rho_P$, $\Delta\rho_V$, $\Delta\rho_D$, $\Delta\rho_{GB}$ are caused by the precipitation in aging, the vacancy, the dislocation, the grain boundary respectively. The most important factor is $\Delta\rho_S$, next is $\Delta\rho_P$, $\Delta\rho_V$, $\Delta\rho_D$, $\Delta\rho_{GB}$ in turn. During solution treatment, Sn atoms are dissolved into the matrix. The dissolution of foreign atoms causes disorder of the α-Mg lattice and an increase in electron scattering, so $\Delta\rho_s$ in the Equation (1) rises. When the solution time exceeds 12 h, the reason for the decrease in resistivity may be due to the decrease of $\Delta\rho_D$ caused by the homogenization of alloy components and the decrease of $\Delta\rho_{GB}$ caused by grain growth during solution treatment.

3.1.2. Microhardness

The relationship between the microhardness and the solution time is shown in Figure 2, which shows that the change in microhardness is related to the change of resistivity, but the trend is the opposite, that is, the hardness decreases with the extension of the solution time. The microhardness remains basically unchanged after 10 h during the solution process.

The microhardness of the solid-solution-treated is lower than that of the as cast sample. It indicates that the Mg_2Sn phase has a strong effect on the matrix. Meanwhile, it reveals the solid-solution strengthening of tin in magnesium is poor because the atom radius of tin is almost the same as that of magnesium.

3.1.3. Microstructure

The microstructure evolution of the Mg-5 wt.%Sn alloys during the solid-solution treatment at different times is shown in Figure 3. The casting structure of the alloy is presented as a dendrite structure, as shown in Figure 3a, and the Mg_2Sn phase precipitate is mainly formed in the interdendrite region.

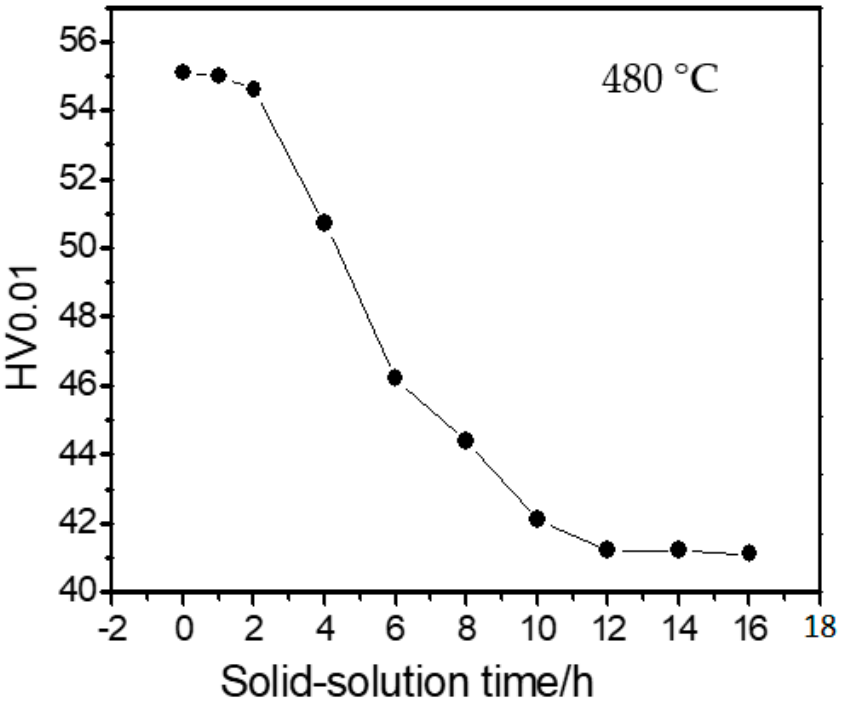

Figure 2. The microhardness of Mg-5 wt.%Sn alloy changes with the solution time during solution treatment at 480 °C.

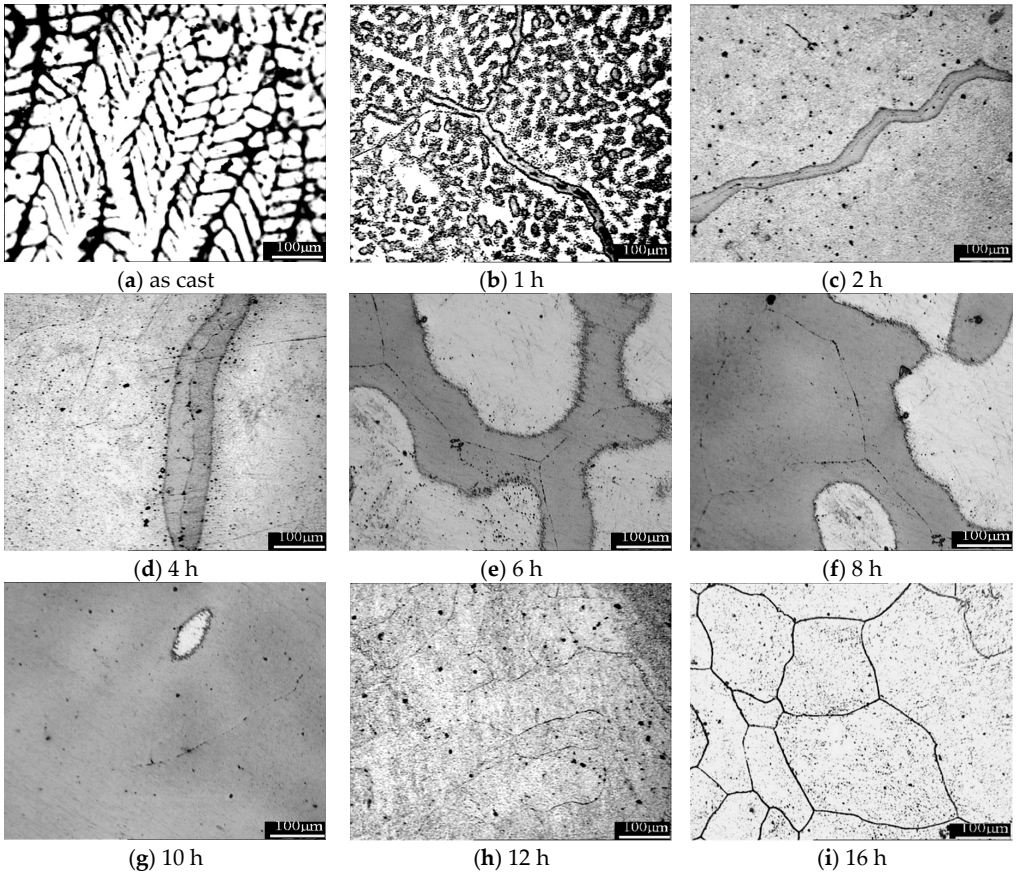

(**a**) as cast (**b**) 1 h (**c**) 2 h

(**d**) 4 h (**e**) 6 h (**f**) 8 h

(**g**) 10 h (**h**) 12 h (**i**) 16 h

Figure 3. Evolution of optical microstructure of Mg-5 wt.%Sn alloy during the solution treatment at 480 °C for different times.

In the solid solution process of Mg-5 wt.%Sn alloy at 480 °C, the secondary dendrite gradually disappears, and the eutectic Mg_2Sn phase gradually dissolves into the α-Mg matrix. After 2 h, the secondary dendrite completely disappeared, and most of the eutectic Mg_2Sn phase dissolved. Interestingly, thin dark gray strips appear around grain boundaries and widen as the solution time increases until the microstructure becomes uniform at 12 h.

To help identify the evolution of microstructure in solution treatment Mg-5 wt.%Sn alloy, we obtained XRD patterns during solution treatment for the different times shown in Figure 4. The peak of Mg_2Sn phase decreases sharply from 1.8% as cast to 0.2% after solution treatment for 1 h, and the XRD pattern changed little from 1 h to 8 h, during which the large size devoiced Mg_2Sn phases dissolve gradually. The peak of Mg_2Sn phase disappear completely until 10 h. From the analysis of the change of electrical resistivity, microhardness of Mg-5 wt.%Sn, and XRD during the solid-solution treatment, the reasonable technique for Mg-5 wt.%Sn alloy should be at 480 °C for 12–16 h. From the comprehensive analysis of the resistivity, microhardness change law and XRD pattern evolution of Mg-5 wt.%Sn alloy during solution treatment, the reasonable process of solution treatment for Mg-5 wt.%Sn alloy should be 12–16 h at 480 °C.

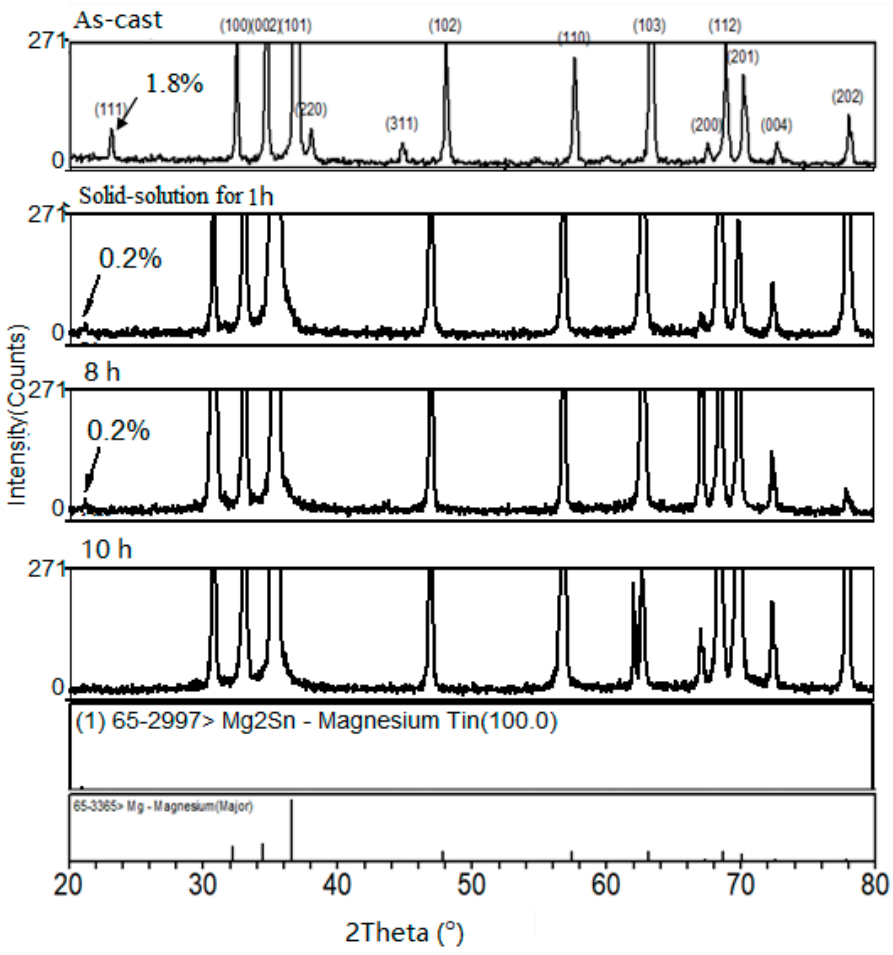

Figure 4. XRD pattern of Mg-5 wt.%Sn under solid-solution treatment at 480 °C for different times.

3.2. Characterization of Aging Process in Mg-5 wt.%Sn Alloy

The optical microscopy microstructures of the supersaturated solid solution of Mg-5 wt.%Sn alloy at different ageing temperatures is shown in Figure 5. Precipitate free zones (PFZ) are found adjacent to the boundary during ageing, so it can be concluded that supersaturated solid solution of Mg-5 wt.%Sn alloy undergoes continuous inhomogeneous precipitation along grain boundaries during aging, and continuous homogeneous precipitation occurs in the matrix.

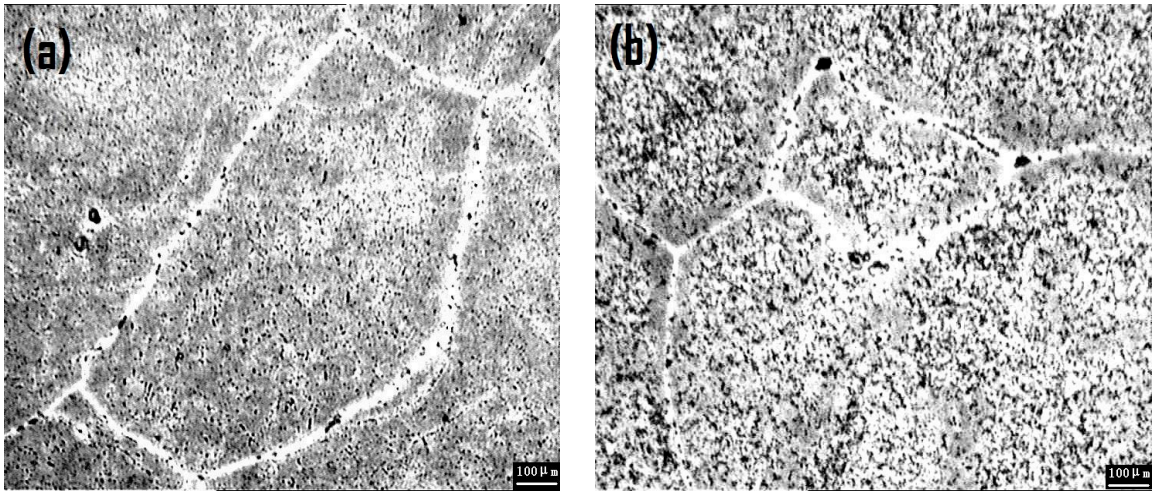

Figure 5. Optical microstructures of the supersaturated solid solution of Mg-5 wt.%wt Sn alloy aged at 160 °C for 720 h (**a**) and 240 °C for 16 h (**b**).

3.2.1. Matrix Precipitates (MPt)

(a) Shape and size of precipitates

Figures 6 and 7 show the shape and size of precipitates aged at 160 °C for 720 h and 240 °C for 16 h respectively. At 160 °C aging treatment for 720 h, the precipitates are predominantly plate-shaped, and at 240 °C aging treatment for 16 h, the precipitates are mainly lath-shaped. The general dimensions of the precipitates for different ageing temperatures and time are given in Table 1. The length and width of the plate-shaped precipitates aged at 160 °C for 720 h are both less than that aged at 240 °C for 16 h, the width of laths aged at 160 °C for 720 h is also less than that aged at 240 °C for 16 h.

Table 1. The size of precipitates in different conditions.

Aging Technique	Precipitates Morphology	Precipitate Size (nm)
160 °C for 720 h	lath-shaped	Width: 51 ± 3
	plate-shaped	Length × Width: 80 (±3) × 130 (±3)
240 °C for 16 h	lath-shaped	Width: 64 ± 5
	plate-shaped	Length × Width: 108 (±5) ×151 (±5)

To distinguish the nature of precipitates, we conducted an EDX analysis were carried out with a beam spot size of 0.5 nm, which indicates that there is enrichment of Sn in precipitates as shown in Table 2. It suggests that the atomic concentration of Sn in precipitates aged at 160 °C for 720 h is among 5–7 at.% which is much less than that of equilibrium Mg_2Sn phase, and in lath-shaped precipitations aged at 240 °C for 16 h is 23.38 at.% which is also less than that of equilibrium Mg_2Sn phase, but in plate-shaped precipitation at 240 °C for 16 h is 30.51 at.% that is near that in the equilibrium Mg_2Sn phase.

Table 2. The composition of the precipitates within grain in different conditions.

Aging Technique	Precipitates Morphology	Mg		Sn	
		wt.%	at%	wt.%	at%
160 °C 720 h	lath-shaped	70.49	96.11	29.51	6.89
	plate-shaped	78.61	94.72	21.39	5.28
240 °C 16 h	lath-shaped	53.77	86.62	46.23	23.38
	plate-shaped	31.25	69.49	68.75	30.51

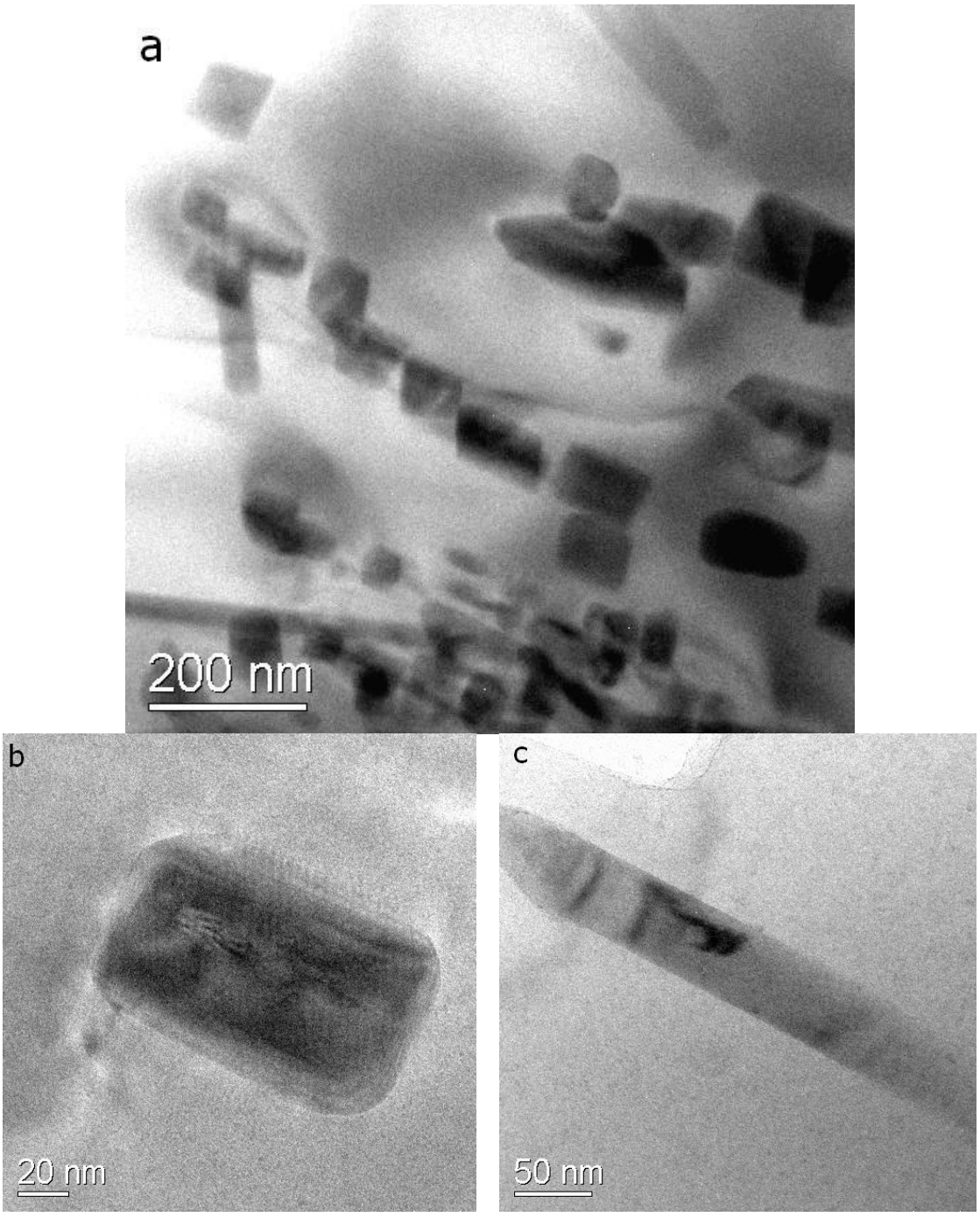

Figure 6. Bright-field TEM micrograph (parallel to $[0001]_{Mg}$) of the precipitates in the supersaturated solid solution of Mg-5 wt.%Sn alloy aged at 160 °C for 720 h (**a**), plate-like morphology (**b**), lath-like morphology (**c**).

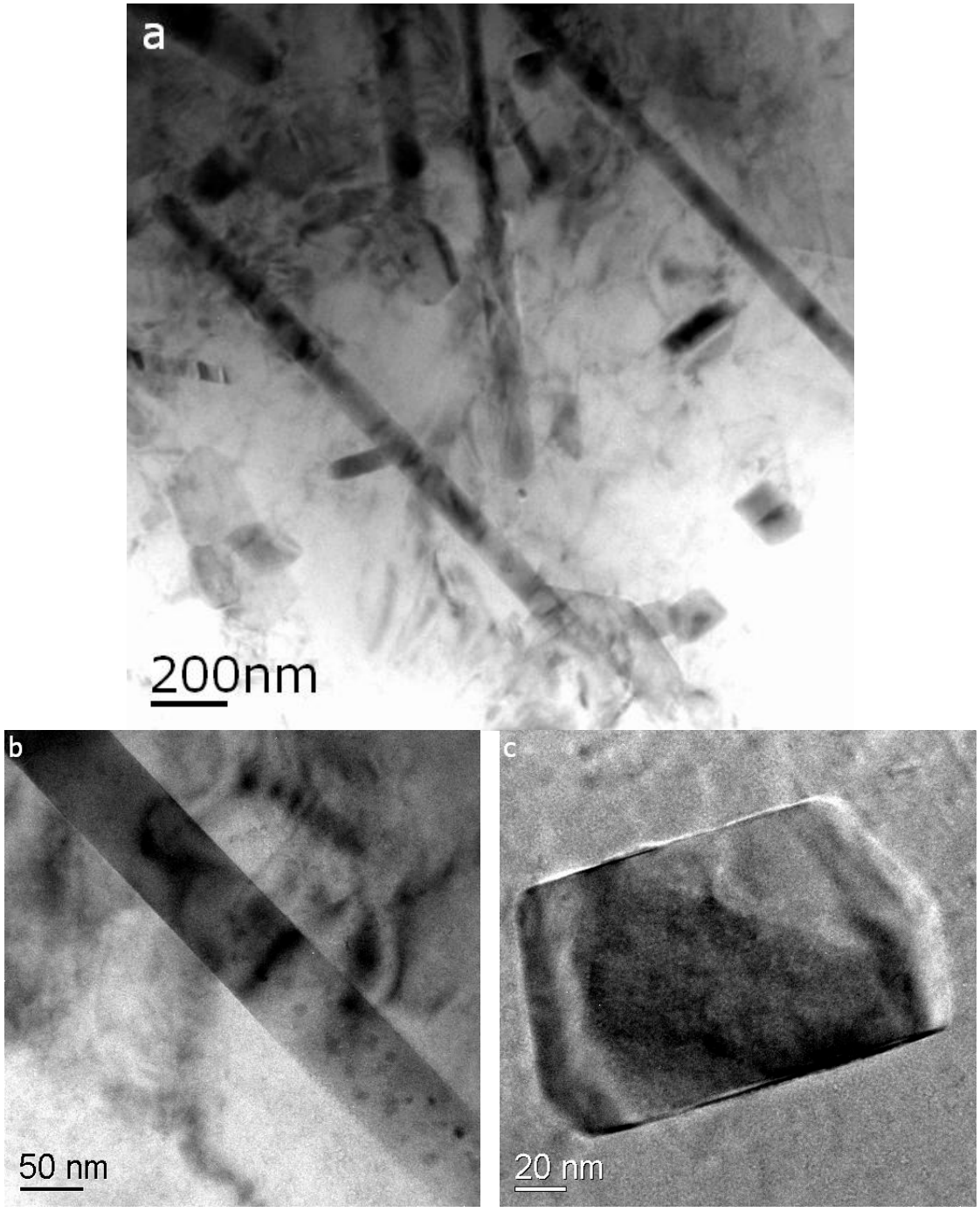

Figure 7. Bright-field TEM micrograph (parallel to $[0001]_{Mg}$) of the precipitates in the supersaturated solid solution of Mg-5 wt.%Sn alloy aged at 240 °C for 16 h (**a**), lath-like morphology (**b**), plate-like morphology (**c**).

(b) The interface of the precipitates with the matrix

HRTEM observations were mainly carried out along the [0001] zone axes of the magnesium matrix, which are suitable to reveal the structural features of the precipitate shown in Figures 8 and 9. This HRTEM image processed by Digital Micrograph includes four procedures: (1) obtain a HRTEM image, (2) make Fast Fourier Transform (FFT), (3) apply mask, and (4) perform inverse FFT.

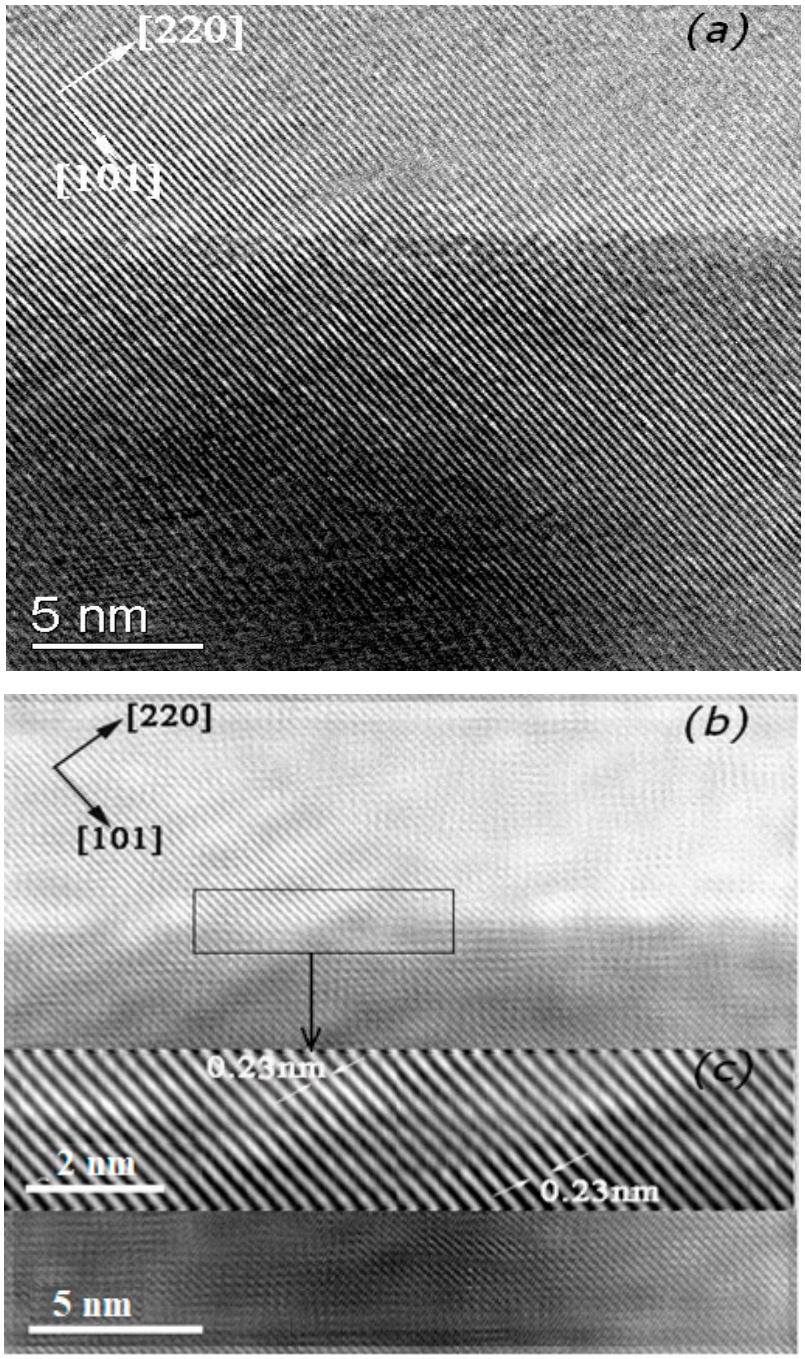

Figure 8. HRTEM image of the interface between lath-shaped precipitate and α-Mg matrix in the supersaturated solid solution of Mg-5 wt.%Sn aged at 160 °C for 720 h (**a**); HRTEM image by the FFT transform (**b**), (**c**) HRTEM image by the FFT transform of the enlarge area in (**b**).

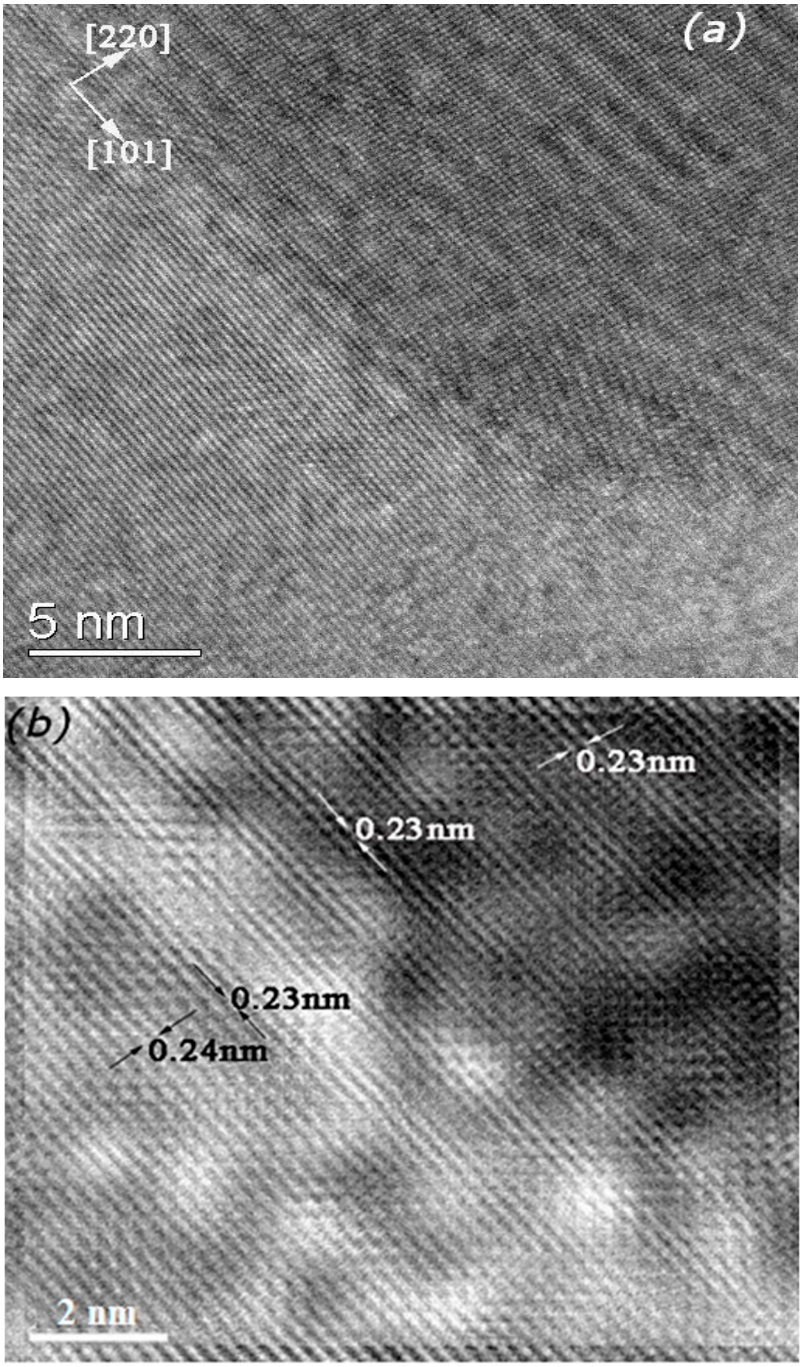

Figure 9. HRTEM image of the interface between plate-shaped precipitate and α-Mg matrix in the supersaturated solid solution of Mg-5 wt.%Sn aged at 160 °C for 720 h (**a**); HRTEM image by the FFT transform (**b**).

Figure 8 indicates that lath-shaped precipitated phase at 160 °C along the [220] zone axis is fully coherent with the matrix along the [101] zone axis. Figure 9 shows the plate-shaped precipitated phase at 160 °C along the [220] zone axis is also fully coherent with the matrix. The (101) lattice plane space of matrix is measured as 0.23~0.24 nm and the (220) lattice plane space of precipitate is measured as 0.23 nm, which approach to their lattice plane parameter ($d^{p}_{[220]}$ = 0.23846 nm, $d^{m}_{[101]}$ = 0.24486 nm), and therefore the interface between the precipitate and the habit plane is highly coherent.

At an ageing temperature of 240 °C for 16 h, the interface between the lath-shaped precipitate and the matrix is semi-coherent shown in Figure 10, and series of edge dislocation

lie on the inter-phase (Figure 10c) to reduce the elastic strain energy. For the plate-shaped precipitate, there is no obvious match relation between the precipitate and the matrix in the parallel (101) direction, and the disordered transitional layered structures emerge at the interface seen in Figure 11.

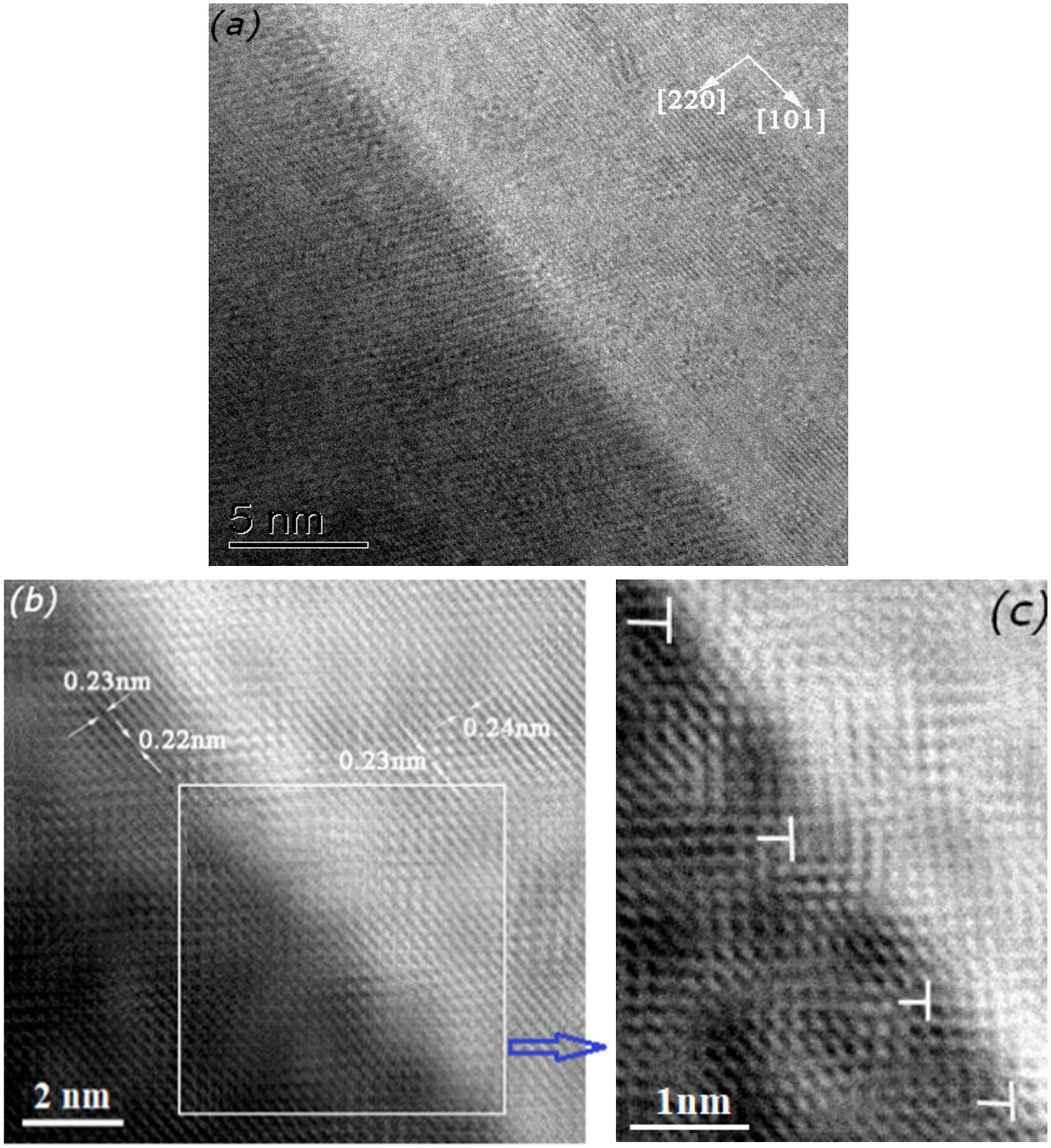

Figure 10. HRTEM image of the interface between lath-shaped morphology precipitates and α-Mg matrix in the supersaturated solid solution of Mg-5 wt.%Sn aged at at 240 °C for 16 h (**a**); HRTEM image by the FFT transform (**b**,**c**).

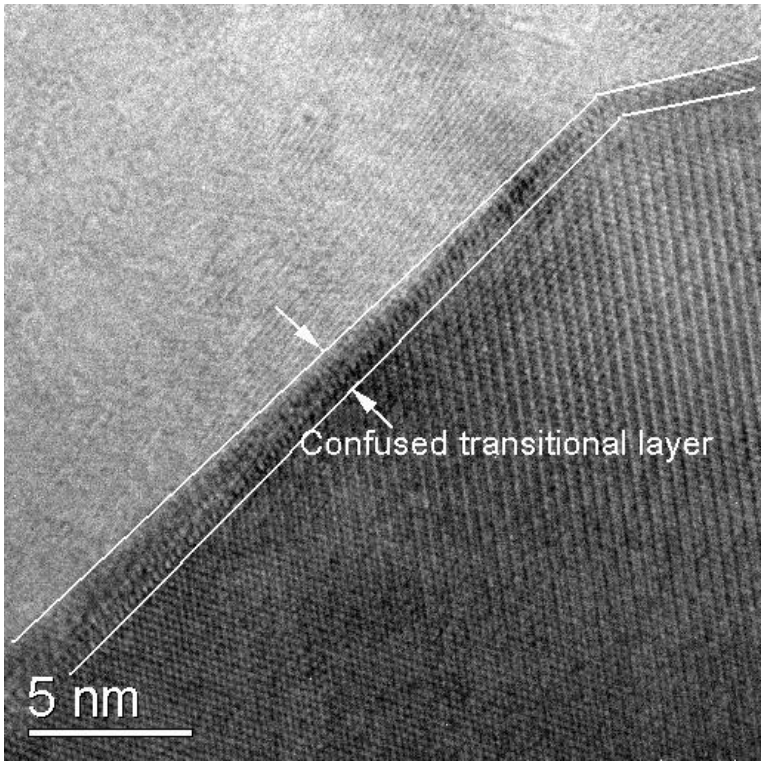

Figure 11. HRTEM image of the interface between plate-shaped morphology precipitates and α-Mg matrix in the supersaturated solid solution of Mg-5 wt.%Sn aged at 240 °C for 16 h.

3.2.2. Grain Boundary Precipitates (GBP)

(a) the shape and size of precipitates

Figure 12 shows TEM images of the precipitates along the [0001] zone axis on the grain boundary in supersaturated solid solution of Mg-5 wt.%Sn alloy aged at 160 °C for 720 h (a) and 240 °C for 16 h (b), respectively. Only plate-shaped precipitates along the grain boundaries are observed during aging, which are slightly bigger in size (seen in Table 3), but fewer in number and more scattered than the precipitates inside the matrix.

Table 3. The size of precipitates at grain boundary in different conditions.

Aging Technique	Precipitate Morphology	Precipitate Size (nm)
160 °C 720 h	plate-shaped	Length × Width: 92 (±5) × 152 (±5)
240 °C 16 h	plate-shaped	Length × Width: 110 (±5) × 155 (±5)

EDX analysis listed in Table 4 indicates that the atomic concentration of Sn in the precipitate aged at 160 °C for 720 h is 20.51 at.% which is still less than that in equilibrium phase of Mg_2Sn. The atomic concentration of Sinn precipitate aged at 240 °C for 16 h is 32.36 at.% that is almost equal to that in equilibrium phase of Mg_2Sn.

Table 4. The component of precipitates at grain boundary in different conditions.

Aging Technique	Precipitate Morphology	Mg		Sn	
		wt.%	at%	wt.%	at%
160 °C 720 h	plate-shaped	44.25	79.49	55.75	20.51
240 °C 16 h	plate-shaped	29.88	67.74	70.12	32.26

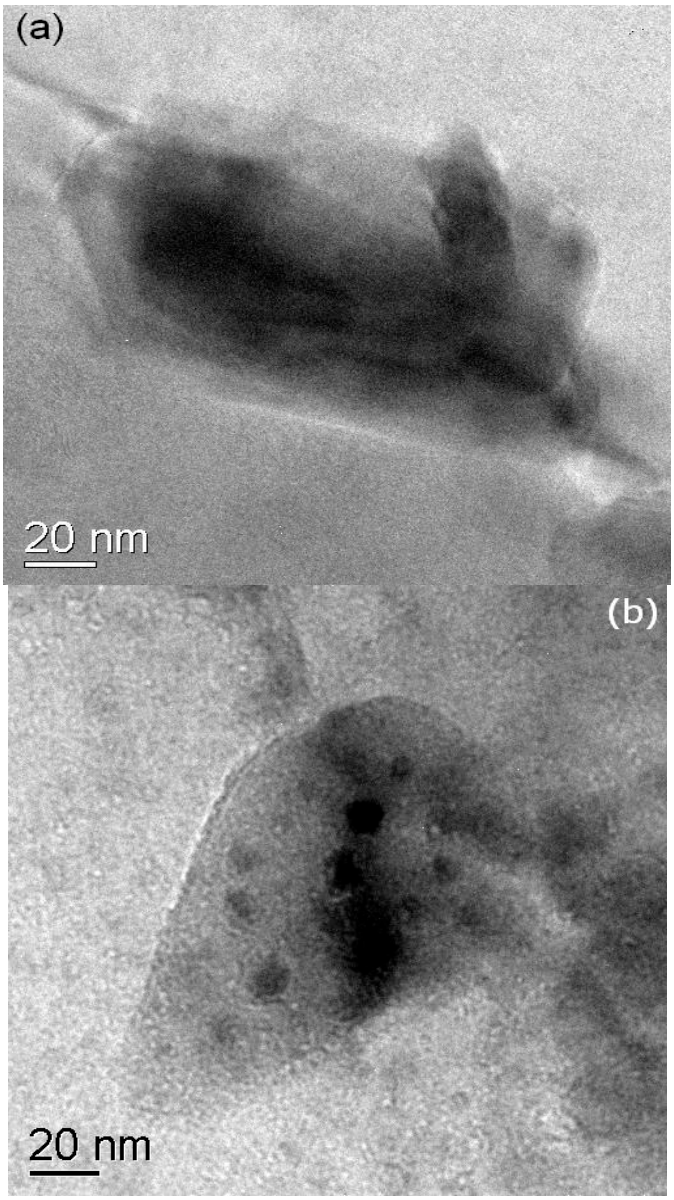

Figure 12. Bright-field TEM micrograph (parallel to $[0001]_{Mg}$) of the precipitates along grain boundary in supersaturated solid solution of Mg-5 wt.% Sn alloy aged at 160 °C for 720 h (**a**) and 240 °C for 16 h (**b**).

3.2.3. The Interface of the Precipitates with Matrix

HRTEM observations were also carried out along the [0001] zone axes of the Mg matrix shown in Figures 13 and 14. Figure 13 indicates that under the condition of 720 h aging at 160 °C, the precipitate along [220] zone axis on the grain boundary is fully coherent with the matrix along the [101] zone axis. The (101) lattice plane space of matrix is measured as 0.24 nm and the (220) lattice plane space of precipitate is measured as 0.24 nm as well. While the precipitate on the grain boundary aged at 240 °C for 16 h is incoherent with matrix, as shown in Figure 14.

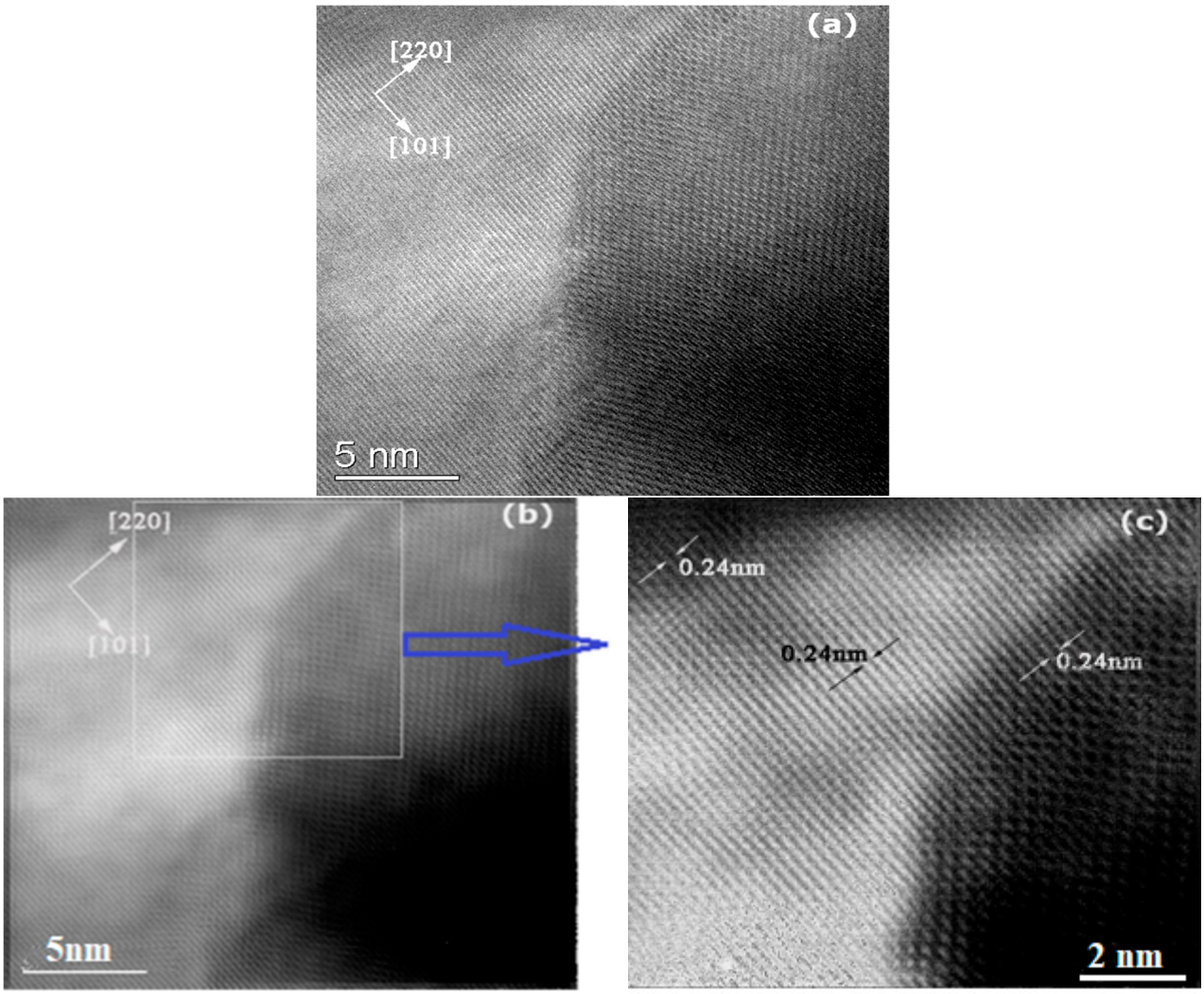

Figure 13. (**a**) HRTEM image of the interface between precipitates at grain boundary and α-Mg matrix in the supersaturated solid solution of Mg-5 wt.%Sn aged at 160 °C for 720 h; HRTEM image by the FFT transform (**b**), (**c**) HRTEM image by the FFT transform of the enlarge area in (**b**).

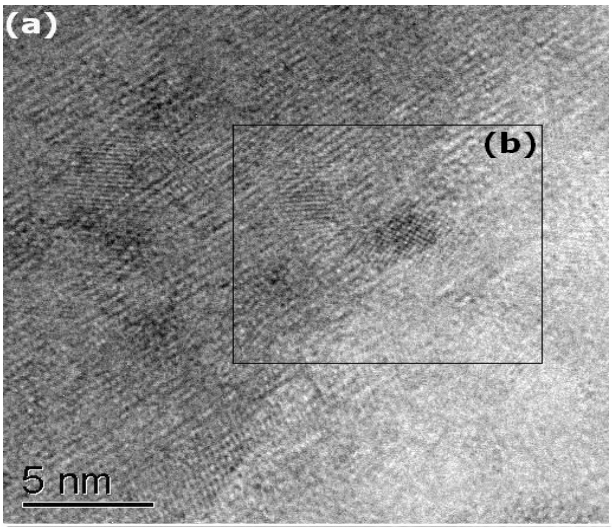

Figure 14. *Cont*.

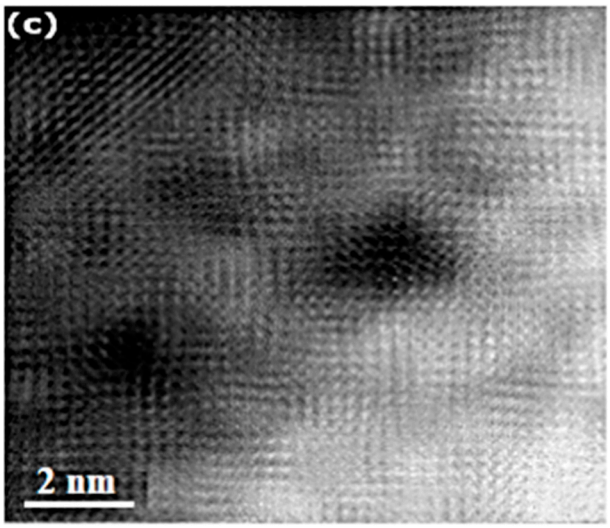

Figure 14. HRTEM image of the interface between precipitates at grain boundary and α-Mg matrix in the supersaturated solid solution of Mg-5 wt.%Sn aged at 240 °C for 16 h (**a**); (**c**) HRTEM image by the FFT transform of the enlarge area (**b**) in (**a**).

4. Discussion

The microstructure evolves during solution-aging. During the solid solution process of Mg-5 wt.%Sn alloy at 480 °C, the secondary dendrite gradually disappears, and the eutectic Mg_2Sn phase gradually dissolves into the α-Mg matrix, and forms supersaturated solid solution. Subsequently, precipitation occurs during the aging process.

The precipitated sequence of the phase depends on the aging temperature. The HRTEM studies indicated a metastable precipitation might occur during ageing in Mg-5 wt.%Sn alloys which lath- or plate-shaped and is coherent or simi-coherent with matrix. EDAX analyses showed that the Sn/Mg ratio in precipitates within grain of Mg-5 wt.%Sn aged at 160 °C for 720 h was not actually constant (5–7 at.%) and much smaller than that of Mg_2Sn equilibrium phase. To help identify these metastable phases, we used an XRD to analyze a supersaturated solid solution of Mg-5 wt.%Sn alloy aged at 160 °C for different times shown in Figure 15. The diffraction peaks of the α-Mg and Mg_2Sn phases can be clearly identified in the as-cast sample, while the diffraction characteristic peaks after solid solution are identified as a single α-Mg phase. It is interesting that a broad diffraction peak on (111) planes of Mg_2Sn emerges at 240 h, which is probably caused by the formation of short-range order, in line with Henes's view [24]. A similar structure was found in Mg-9.8 wt.%Sn aged at 100 °C for 2056 h [25], which was confirmed to be GP zone [25]. The GP zone was lath-shaped with a habit plane parallel to the basal plane [25].

The intensity of the broad diffraction peak decreases steady with ageing time and on its right side ($2\theta = 22.9°$) the weak (111) diffraction peak appears. With the further increase of aging time, the intensity of (111) diffraction peak phase is further enhanced. The XRD analysis results confirm the existence of the metastable phases. The study [26] on Mg-9.8 wt.%Sn and has revealed that a metastable phase β′ occured before the formation of the equilibrium β phase (Mg_2Sn, FCC, a = 0.6760 nm) aged in the temperature range 100–250 °C. The metastable phase has a $L1_2$ structure (space group Pm3m, lattice parameter a = 0.453 nm) and a Mg_3Sn composition. The β′ phase is fully coherent with the magnesium matrix in its the habit plane. The Mg_3Sn metastable phase has confirmed in Mg-7 wt.%Sn aged at 220 °C for 12 h by the L. Tong et al. [26].

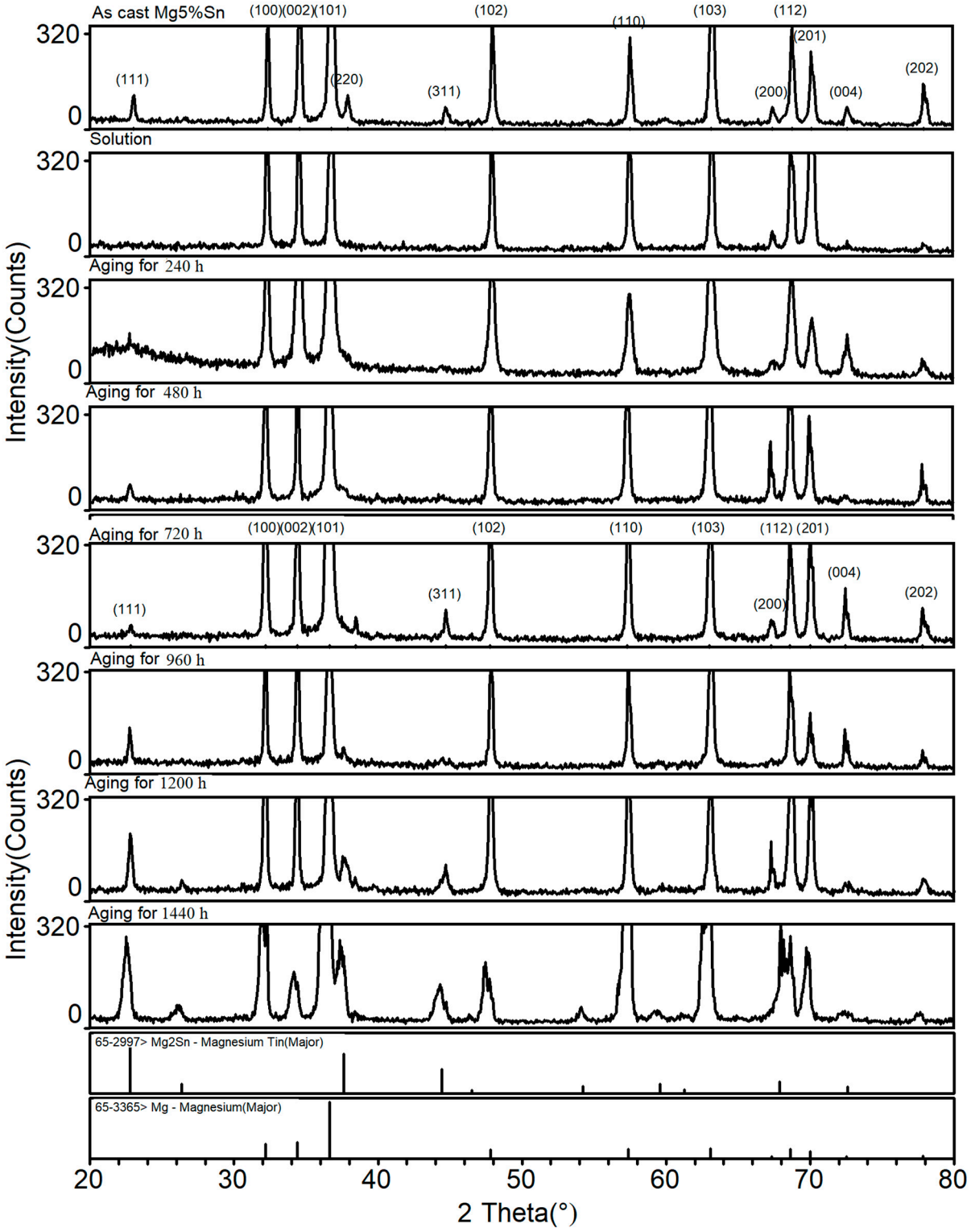

Figure 15. XRD patterns of the supersaturated solid solution of Mg-5 wt.%Sn aged at 160 °C for different times.

Our experimental results in Tables 2 and 4 show that the Mg/Sn ratio of coherent precipitates is 5–7 at.% which is much less than that of the Mg_3Sn phase (Mg/Sn ratio should be around 25 at.%), indicating GP zone form in Mg-5 wt.% alloy aged at 160 °C. Therefore, the precipitated sequence of the phase is as follows, supersaturated solid solution → GP zone →β′ (Mg_3Sn) → β (Mg_2Sn) in the aging process at 160 °C.

The semi-coherent precipitates has Mg/Sn ratio is 23.38 at.% as shown in Figure 10 and Table 4, very close to that of Mg_3Sn phase, confirming that the Mg_3Sn metastable phase does form before the formation of the equilibrium Mg_2Sn phase aged at 240 °C. Therefore, the precipitated sequence of the phase is as following, supersaturated solid solution → β′ (Mg_3Sn) → β (Mg_2Sn) in the aging process at 240 °C. During the aging process at 240 °C, no GP zone is found due to the increase in aging temperature, where the β′ (Mg_3Sn) phase is directly formed. In addition, the interface between the β phase and the matrix is semi-coherent aging at 240 °C. At the same time the interface between the β phase and the matrix is completely coherent aging at 160 °C.

5. Conclusions

(1) Through the analysis in the changes of resistivity and microhardness of Mg-5 wt.%Sn during solution treatment, it is proposed that a reasonable solution treatment process should be kept at 480 °C for 12–16 h.

(2) The supersaturated solid solution of Mg-5 wt.%Sn alloy decomposes during ageing. Continuous inhomogeneous precipitation happens along grain boundary and the continuous homogeneous precipitation occurs within grain.

(3) The plate- and lath-shaped precipitates are observed within the grains in aged Mg-5 wt.%Sn alloy.

For those precipitations aged at 160 °C for 720 h, EDX analysis suggests that the atomic concentration of Sn is from 5 to 7 at.%, which is much less than that of Mg_2Sn equilibrium phase, and HRTEM analysis indicates that the interface between the precipitate and matrix is coherent.

For those precipitations aged at 240 °C for 16 h, the atomic concentration of Sn in the lath-shaped precipitate is 23.38 at.%, and the interface between the lath-shaped precipitate and matrix is semi-coherent. At the same time the atomic concentration of Sn in the plate-shaped precipitate is 30.51 at.% that is close to that of Mg_2Sn equilibrium phase, and the interface between plate-shaped precipitate and matrix is non-coherent.

(4) Only the plate-shaped precipitates along the grain boundaries were observed in aged Mg-5 wt.%Sn alloy. EDX analysis indicates that the atomic concentration of Sn in the precipitates is 20.51 at.% aged at 160 °C for 720 h and 32.26 at.% aged at 240 °C for 16 h respectively, and the interfaces between the precipitates and the matrix are coherent at 160 °C for 720 h, but non-coherent at 240 °C for 16 h.

(5) GP zones and metastable Mg_3Sn phase form in Mg-5 wt.% alloy aged at 160 °C, while only metastable Mg_3Sn phase was discovered in the Mg-5 wt.% alloy aged at 240 °C. The precipitated sequence of the phase is as follows, supersaturated solid solution → GP zone → β′ (Mg_3Sn) → β (Mg_2Sn) in the aging process at 160 °C, while the precipitated sequence of the phase is as follows, supersaturated solid solution → β′ (Mg_3Sn) → β (Mg_2Sn) in the aging process at 240 °C.

Author Contributions: Y.L.: Methodology, Theoretical Calculations, All Data Graphs, Critical Analysis, Investigation, Drafting. H.L.: Conceptualization, Methodology, Critical Analysis, Investigation, Writing. All authors have read and agreed to the published version of the manuscript.

Funding: This research received no external funding.

Data Availability Statement: The data that support the findings of this study are available from the corresponding authors upon reasonable request.

Conflicts of Interest: The authors declare no conflict of interest. All authors are aware of the manuscript and have given almost equal contributions to the research.

References

1. Deng, Y.; Sun, W.; Yang, Y.; Zhan, H.; Yan, K.; Zeng, G. Effects of Mg_2Sn precipitation on the age-hardening and deformation behaviour of a Mg-Sn-Al-Zn alloy. *Mater. Sci. Eng. A* **2023**, *867*, 144714. [CrossRef]
2. Gibson, M.; Fang, X.; Bettles, C.; Hutchinson, C. The effect of precipitate state on the creep resistance of Mg-Sn alloys. *Scr. Mater.* **2010**, *63*, 899–902. [CrossRef]

3. Zhao, C.; Chen, X.; Pan, F.; Gao, S.; Zhao, D.; Liu, X. Effect of Sn content on strain hardening behaviour of as-extruded Mg-Sn alloys. *Mater. Sci. Eng. A* **2018**, *713*, 244–252. [CrossRef]
4. Hasani, G.H.; Mahmudi, R. Tensile properties of hot rolled Mg–3Sn–1Ca alloy sheets at elevated temperatures. *Mater. Design* **2011**, *32*, 3736–3741. [CrossRef]
5. Zhao, Z.; Bai, P.; Guan, R.; Murugadoss, V.; Liu, H.; Wang, X.; Guo, Z. Microstructural evolution and mechanical strengthening mechanism of Mg_3Sn-1Mn-1La alloy after heat treatments. *Mater. Sci. Eng. A* **2018**, *734*, 200–209. [CrossRef]
6. Fu, J.; Yang, Y. Formation of the solidified microstructure in Mg-Sn binary alloy. *J. Cryst. Growth* **2011**, *322*, 84–90. [CrossRef]
7. Rao, K.P.; Suresh, K.; Prasad, Y.V.R.K.; Hort, N.; Kainer, K.U. Forging of cast Mg-3Sn-2Ca-0.4Al-0.4Si magnesium alloy using processing map. *J. Mech. Sci. Technol.* **2016**, *30*, 2699–2705. [CrossRef]
8. Dharmendra, C.; Rao, K.P.; Suresh, K.; Hort, N. Hot deformation behaviour and processing map of Mg-3Sn-2Ca-0.4Al-0.4Zn alloy. *Metals* **2018**, *8*, 216. [CrossRef]
9. Zhao, Z.; Guan, R.; Zhang, J.; Zhao, Z.; Bai, P. Effects of process parameters of semisolid stirring on microstructure of Mg–3Sn–1Mn–3SiC (wt.%) strip processed by rheo-rolling. *Acta Metall. Sin. (China)* **2017**, *30*, 66–72. [CrossRef]
10. Zhao, C.; Pan, F.; Zhao, S.; Pan, H.; Song, K.; Tang, A. Microstructure, corrosion behaviour and cytotoxicity of biodegradable Mg-Sn implant alloys prepared by sub-rapid solidification. *Mater. Sci. Eng. C* **2015**, *54*, 245–251. [CrossRef]
11. Zhao, C.; Pan, F.; Zhao, S.; Pan, H.; Song, K.; Tang, A. Preparation and characterization of as-extruded Mg-Sn alloys for orthopaedic applications. *Mater. Design* **2015**, *70*, 60–67. [CrossRef]
12. Kim, D.H.; Lee, J.Y.; Lim, H.K.; Kyeong, J.S.; Kim, W.T. The Effect of Microstructure Evolution on the Elevated Temperature Mechanical Properties in Mg-Sn-Ca System. *Mater. Trans.* **2008**, *49*, 2405–2413. [CrossRef]
13. Hort, N.; Huang, Y.; Abu Leil, T.; Maier, P.; Kainer, K.U. Microstructural Investigations of the Mg-Sn-xCa System. *Adv. Eng. Mater.* **2006**, *8*, 359–364. [CrossRef]
14. Mendis, C.; Bettles, C.; Gibson, M.; Hutchinson, C. An enhanced age hardening response in Mg-Sn based alloys containing Zn. *Mater. Sci. Eng. A* **2006**, *435–436*, 163–171. [CrossRef]
15. Sasaki, T.T.; Oh-ishi, K.; Ohkubo, T.; Honoa, K. Enhanced age hardening response by the addition of Zn in Mg-Sn alloys. *Scr. Mater.* **2006**, *55*, 251–254. [CrossRef]
16. Cohen, S.; Goren-Muginstein, G.R.; Avraham, S. *Magnesium Technology 2004*; Alan, A.L., Ed.; TMS (The Minerals, Metals & Materials Society): Pittsburgh, PA, USA, 2004; pp. 301–305.
17. Xiao, W.; Jia, S.; Wang, L.; Wu, Y.; Wang, L. Effects of Sn content on the microstructure and mechanical properties of Mg–7Zn–5Al based alloys. *Mater. Sci. Eng. A* **2010**, *527*, 7002–7007. [CrossRef]
18. Liu, H.; Chen, Y.; Tang, Y. The microstructure, tensile properties, and creep behavior of as-cast Mg–(1–10)% Sn alloys. *J. Alloys Compd.* **2007**, *440*, 122–126. [CrossRef]
19. Liu, H.; Chen, Y.; Tang, Y. The microstructure and mechanical properties of permanent-mould cast Mg-5 wt.% Sn–(0–2.6) wt.% Di alloys. *Mat. Sci. Eng. A* **2006**, *437*, 348–355. [CrossRef]
20. Liu, H.; Chen, Y.; Tang, Y. Tensile and indentation creep behavior of Mg–5% Sn and Mg–5% Sn–2% Di alloys. *Mat. Sci. Eng. A* **2007**, *464*, 124–128. [CrossRef]
21. Derge, G.; Kommel, A.R.; Mehl, R.F. Studies upon the Widmanstatten structure IX—The Mg–Mg_2Sn and Pb–Sb systems. *Trans. AIME* **1937**, *124*, 367.
22. Van Der Planken, J. Precipitation hardening in magnesium-tin alloys. *J. Mater. Sci.* **1969**, *4*, 927–929. [CrossRef]
23. Henes, S.; Gerold, V. Roentgenographic investigation of the separation processes in magnesium-lead and magnesium-zinc alloys. ii. the separation of the stable equilibrium phase. *Metallk* **1962**, *53*, 743.
24. Liu, C.; Chen, H.; Liu, H.; Zhao, X.; Nie, J. Metastable precipitate phases in Mg-9.8 wt% Sn alloy. *Acta Mater.* **2018**, *144*, 590–600. [CrossRef]
25. Tong, L.; Jiang, J.; Bi, G.; Xu, Z.; Li, Y.; Chen, T.; Chen, T.; Zhang, X.; Fu, W.; Fang, D. Remarkable age-hardening response and microstructural evolution of Mge7Sn alloy. *J. Mater. Sci.* **2023**, *24*, 1442–1453.
26. Luo, Z.; Chen, X.; Song, K.; Liu, C.; Dai, Y.; Zhao, D.; Pan, F. Efect of Alloying Element on Electromagnetic Interference Shielding Efectiveness of Binary Magnesium Alloys. *Acta Metall. Sin.* **2019**, *32*, 817–824. [CrossRef]
27. Pan, H.; Pan, F.; Yang, R.; Peng, J.; Zhao, C.; She, J.; Gao, Z.; Tang, A. Thermal and electrical conductivity of binary magnesium alloys. *J. Mater. Sci.* **2014**, *49*, 3107–3312. [CrossRef]
28. Raeisinia, B.; Poole, W.J.; Lloyd, D.J. Examination of precipitation in the aluminum alloy AA6111 using electrical resistivity measurements. *Mater. Sci. Eng. A* **2006**, *420*, 245–249. [CrossRef]